THE ASTROPHYSICAL JOURNAL, 274:698–716, 1983 November 15

THE DISCOVERY OF NEW EMBEDDED SOURCES IN THE CENTRALLY CONDENSED CORE OF THE RHO OPHIUCHI DARK CLOUD: THE FORMATION OF A BOUND CLUSTER?

BRUCE A. WILKING
Department of Planetary Sciences, Lunar and Planetary Lab, University of Arizona, Tucson
AND
CHARLES J. LADA[1]
Steward Observatory, University of Arizona, Tucson
Received 1982 August 2; accepted 1983 April 22

ABSTRACT

New and extensive millimeter-wave and near-infrared observations of the central regions of the ρ Oph cloud are presented. Well-sampled $C^{18}O$ observations have revealed a 1×2 pc ridge which forms the centrally condensed core of the ρ Oph cloud. Extremely large gas and dust column densities prevail in this core: $N^{18}_{\rm LTE} = 1.4\text{–}2.9 \times 10^{16}$ cm^{-2} and $A_v = 50\text{–}106$ mag. A cloud mass of 550 $M_\odot$ is obtained for the area mapped. A completely sampled 2 μm survey to a limiting magnitude of $K = +12.0$ mag was conducted in a 105 arcmin^2 box centered on the region of highest extinction, as indicated by our $C^{18}O$ observations. This survey and subsequent J, H, K, L photometry have resulted in the discovery of a population of 20 objects embedded in the dense, central region of the ρ Oph cloud.

The synthesis of these new data with those of previous investigators enables us to place important constraints on the size and nature of the embedded stellar population and on the star formation process in the cloud. In particular, we are able to calculate a star formation efficiency (SFE) for the central core of the cloud. We find the SFE to be between 34%–47% in the limiting cases that the embedded population is primarily composed of low-luminosity pre–main-sequence stars and of early-type zero-age main-sequence (ZAMS) stars, respectively. It is shown that if the SFE exceeds 50% before the molecular gas is disrupted and dispersed, then a gravitationally bound cluster will emerge from a molecular cloud. Considering the relatively quiescent conditions in the ρ Oph molecular gas, our data suggest that the formation of a bound cluster in the ρ Oph cloud is imminent. The combination of our millimeter-wave and near-infrared data allows us to estimate that the total stellar mass of this cluster is between 135 and 240 $M_\odot$, depending on whether the members are primarily low-luminosity or ZAMS stars, respectively. However, comparison of near-infrared and far-infrared data strongly suggests the cluster is predominantly composed of low-luminosity stars which may still be contracting toward the main sequence.

Subject headings: clusters: open — nebulae: individual — stars: formation

I. INTRODUCTION

There are 63 optically identified open clusters within 750 pc of the Sun (Mermilloid 1980). Most of these objects are stellar groups which appear to have lifetimes as gravitationally bound systems on the order of 3×10^8 yr (Wielen 1971). The formation of such bound clusters from molecular clouds is an interesting problem, particularly since most stars are believed to have formed in unbound associations (Roberts 1957). Associations themselves form in giant molecular clouds where the conversion efficiency of gaseous to stellar mass is observed to be low (e.g., Duerr, Imhoff, and Lada 1982), a condition not conducive to the formation of a bound stellar system (Hills 1980). What are the circumstances that make it possible for star formation to result in the production of a bound, rather than unbound, stellar system from a molecular cloud? Progress toward answering this fundamental question would be greatly facilitated by the identification of a young cluster or protocluster still embedded within a molecular cloud. Studies of the nearby Pleiades open cluster suggest that star formation in this bound stellar aggregate was a continuous process lasting perhaps as long as 100 million years (Herbig 1962; Landolt 1979; Stauffer 1980). If this suggested duration of star formation is similar for all open clusters, then such clusters may spend as much as 30% of their total lifetimes buried in their parental molecular clouds. Consequently, considering the number of optical open clusters in the solar neighborhood, we estimate that 31 buried open clusters may exist within

[1]Alfred P. Sloan Foundation Fellow.

750 pc of the Sun, and these clusters may still be forming stars.

Unfortunately, there has yet to be a positive identification of a star-forming region which is producing a future bound stellar system. Recognition of such a region would clearly enable us to begin investigations of the star formation process which results in formation of a bound stellar group. In particular, we would be able to study the physical conditions in the molecular gas, which ultimately must determine the nature of the stellar system being produced.

In principle, the single most useful parameter which can be used to distinguish between a protocluster and protoassociation is the star formation efficiency, defined as the ratio of the total mass of stars to the total mass of molecular gas plus stars within a star-forming volume. As shown in § V, for an initially virialized cloud, a bound cluster will be produced only if the star-forming efficiency within the volume of gas creating stars exceeds 50% before the gas is disrupted and expelled by stellar winds, H II regions, and supernovae, which are likely to occur after the stars are formed (see also Hills 1980). Protocluster molecular clouds may not be initially virialized, and even higher star formation efficiencies would be required (Hills 1980). Nonetheless, if a cloud could be identified with an efficiency as high as 50%, it would be a prime candidate for cluster formation. Unfortunately, evaluating the star-forming efficiency in a specific molecular cloud is exceedingly difficult since knowledge of both the gaseous and stellar masses is required for a well-defined cloud volume, yet, most of the stars will be buried within the cloud and heavily obscured.

One of the best candidates for a protocluster region is the ρ Ophiuchi dark cloud. The ρ Oph cloud lies in the Sco-Cen OB association at a distance of only 160 pc (Bok 1956; Bertiaud 1958; Whittet 1974). The dark cloud is regarded as a site of recent star formation because of its relationship to nearby early-type stars, numerous embedded infrared sources (Grasdalen, Strom, and Strom 1973; Vrba *et al.* 1975; Elias 1978), and enhanced molecular emission from numerous molecular species (e.g., Myers *et al.* 1978). Because of the high density of 2 μm sources detected toward this cloud, Grasdalen, Strom, and Strom have suggested it is the site of the formation of an open cluster. The proximity of the ρ Oph cloud enables the study of its embedded population and the conditions in the star-forming molecular gas with a fine detail matched by only a few complexes.

Although the ρ Oph cloud and embedded population are well studied, not enough information exists to be able to evaluate the star formation efficiency with any certainty. Our ignorance of such basic information as the true gas column density distribution in the cloud and the numbers and masses of the embedded sources in ρ Oph was brought to light by the discovery of ^{13}CO self-absorption by Lada and Wilking (1980). Figure 1 shows high velocity resolution ^{12}CO, ^{13}CO, and $^{12}C^{18}O$ (hereafter $C^{18}O$) profiles toward the position of ρ Oph where ^{13}CO self-absorption was originally detected. The symmetry of the $C^{18}O$ line relative to the ^{13}CO profile suggests that ^{13}CO emission is optically thick, and that previous mass determinations based upon ^{13}CO studies in ρ Oph are probably not reliable. In addition, surprisingly few near-infrared sources have been observed toward the regions of the cloud where the ^{13}CO self-absorption is most prominent and the gas column densities and visual extinctions are the greatest. Evidently previous near-infrared surveys were not sensitive enough to completely sample the embedded population in the high-extinction areas of ρ Oph.

In order to determine the star formation efficiency in ρ Oph and the likelihood of the formation of a bound stellar system from this cloud, two sets of detailed observations were needed. First, a thorough mapping of the central regions of the complex in an optically thin CO line (i.e., $C^{18}O$) was necessary to identify the regions of highest extinction and to discover the true magnitude

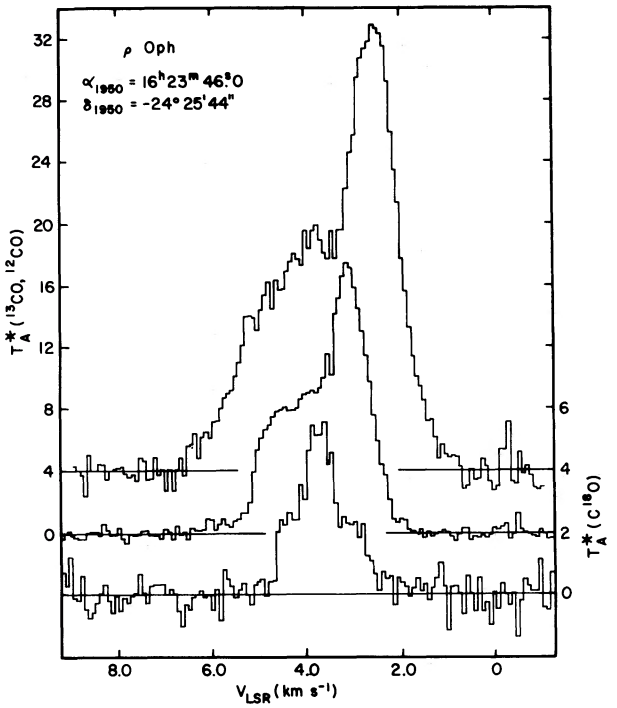

FIG. 1.—High-resolution (30 kHz) ^{12}CO, ^{13}CO, and $C^{18}O$ profiles toward the 3E 9S position in the ρ Oph cloud. These observations were made with the NRAO 11 m telescope operating in the position-switched mode with an off-position 60′ south of our reference position (source 1). Absolute calibration of T_A^* was established by observing either IRC +10216 (Ulich and Haas 1976) or M17 SW (Lada 1976) as standards. The ^{12}CO and ^{13}CO emission lines are self-absorbed on the high-velocity side of the line as indicated by the symmetry of the $C^{18}O$ line.

of the hydrogen column densities in these regions. Second, a deeper, completely sampled near-infrared survey of the central cloud regions plus extensive photometry of any discovered sources was needed to estimate accurately the number of embedded stars and, if possible, their masses.

This paper describes such a coordinated and extensive millimeter-wave and near-infrared study of the ρ Oph cloud. We have performed this study in order to obtain the data base necessary for both an estimation of the star-forming efficiency in the cloud as well as a detailed investigation of the star formation process in this region. In § II, we describe our millimeter-wave and near-infrared observing procedures. In § III*a*, we use our millimeter-wave $C^{18}O$ spectral-line observations to determine the distribution of gas column densities and to estimate the total mass of the cloud. Section III*b* draws upon both infrared and $C^{18}O$ data to determine which sources that were discovered in the course of our 2 μm survey are likely to be embedded in the cloud. The synthesis of our infrared data with previously published near-infrared, far-infrared, radio continuum, and optical data is the topic of § IV. This allows us to estimate the numbers and masses of embedded stars within the core region of the cloud as defined by our $C^{18}O$ observations. In § IV*a*, we identify an embedded population of 44 observable objects within the ρ Oph core region. Section IV*b* describes luminosity and mass estimates made for these objects for two limiting cases: (1) the sources are early-type zero-age main-sequence (ZAMS) in nature, and (2) the objects are primarily low-luminosity objects which may still be contracting toward the main sequence. In both instances, we can obtain the extinction through, or depth into, that part of the cloud within which all sources are observed. This, in turn, enables a determination of the mass of gas in this layer which is coexistent with the embedded stars and of the star formation efficiency in this volume.

The resulting star-forming efficiencies are calculated in § V and found to be 34% and 47% for an intrinsically low-mass population and a ZAMS population, respectively. The implications of these high efficiencies are discussed in the framework of the formation of bound stellar systems. With the aid of our $C^{18}O$ observations, estimates of the total size and mass of the embedded cluster are made and compared with known open cluster systems.

II. OBSERVATIONS

a) *The* $C^{18}O$ *Observations*

The $C^{18}O$ observations were obtained in May of 1980 with the NRAO 11 m telescope located at Kitt Peak.[2] Spectra were acquired with the cooled, Cassegrain, dual-channel mixer receiver. A 128 channel filter-bank spectrometer with 100 kHz resolution was used for each polarization channel. This translates into a velocity resolution of 0.27 km s^{-1} for the $J = (1 \rightarrow 0)$ transition of $C^{18}O$. The spectral line was positioned in each polarization channel such that the background could be subtracted by frequency-switching across one-half of the total bandwidth. The data from each polarization channel were averaged together and folded to produce the final spectral-line profile. By operating in the frequency-switched mode with both polarization channels, high-quality spectra were obtained with 3 minute integrations. This high degree of sensitivity allowed us to observe 360 points over the central regions of the ρ Oph dark cloud with our 1.′1 beam. The spatial coverage of these observations is shown in Figure 3.

Temperature scales were established using a rotating ambient absorber. Final calibration was achieved by repeated observations of the 3E 9S[3] position in the ρ Oph cloud in the course of a single night. The absolute calibration of the antenna temperature, T_A^*, at the 3E 9S position was established both from observations made with a mesh filter which minimizes the effect of the image sideband and from comparison with M17 SW, assuming T_A^*(M17 SW) = 2.0 K (Lada 1976). As a result, we adopted a mean value of T_A^*(3E 9S) = 4.84 $\pm$ 0.09 K. From the repeated observations of the standard position we estimate the uncertainty in T_A^* for a single integration to be about 10%.

In order to convert antenna temperature to brightness temperature, T_B, it is necessary to correct T_A^* for the forward beam coupling efficiency, η_f, which is not accounted for in the chopper wheel calibration. This efficiency factor can be estimated utilizing knowledge of the antenna power pattern and the source brightness distribution (see Ulich and Haas 1976 for complete description). Assuming a symmetric Gaussian source brightness distribution with a width of 7′ (as determined from our observations) and parameters appropriate for the 11 m telescope, we derive an efficiency factor of $\eta_f = 0.78$. Brightness temperatures are then obtained by dividing the antenna temperatures by 0.78.

b) *The Near-Infrared Observations*

Using our $C^{18}O$ observations as a guide, we selected a 10′ × 10.′5 (0.5 × 0.5 pc) box which enclosed the most extensive area of strong $C^{18}O$ emission and, by implication, the highest visual extinctions for our sensitive 2 μm survey. This 2 μm survey was conducted with the University of Arizona 1.54 m telescope in May of 1980 using a liquid-He–cooled photovoltaic InSb detector (refer to Rieke *et al.* 1981 for details of the detector). The instantaneous 3:1 signal-to-rms noise for the 2 μm

[2]The National Radio Astronomy Observatory is operated by Associated Universities, Inc., under contract with the National Science Foundation.

[3]All offsets are computed in arcmin steps from source 1 ($\alpha_{1950} = 16^h23^m32^s.8$, $\delta_{1950} = -24°16'44''$).

survey was always better than 12.1 mag. The 12″ beam was scanned in right ascension at a rate of about 5″ s^{-1} while chopping to a reference beam 15″ away in R.A. The scans were separated by half the beam size in declination, resulting in complete sampling of the surveyed area.

Subsequent J (1.25 μm), H (1.6 μm), K (2.2 μm), and 3.4 μm photometric observations were performed for the sources detected in the 2 μm survey with the same detector using both the University of Arizona's 2.3 m and 1.54 m telescopes. The photometric observations utilized the standard procedure as described by Low and Rieke (1974). 22 Sco was observed 3–4 times each night to serve as the photometric standard (Harris, Woolf, and Rieke 1978). The photometric observations were made with an 8″ beam on the 2.3 m telescope and a 12″ beam on the 1.54 m.

Source positions and colors obtained for the 20 objects detected in this 2 μm survey are presented in Table 1. Except where noted in Table 1, observations were made with the 1.54 m telescope. For two objects, numbers 13 and 15, the J, H and J, H, 3.4 μm colors, respectively, are those previously obtained by Elias (1978). Errors accompanying the photometry are typically the statistical one sigma errors encountered in the actual flux measurement. Systematic errors which may have occurred due to changes in the atmospheric transparency or equipment response are reflected in the standard star observations and are added quadratically to the statistical errors when they are found to be comparable.

The distribution of the 20 infrared sources is shown in Figure 2. As a result of previous 2 μm surveys of the area by Grasdalen, Strom, and Strom (1973, hereafter GSS), Vrba *et al.* (1975, hereafter VSSG), and Elias (1978), we anticipated four of these objects. They are identified in Table 1—objects 4 (VS-26), 10 (object A from VSSG), 13 (VS-25), and 15 (EL-29). Four previously undetected objects were detected with $K < 10$ mag and are within the area surveyed by VSSG. The coordinates given for VS-30 and VS-31 by VSSG would place both sources in our survey box. Although we detected objects in their vicinity, these objects are fainter than the limiting magnitude of VSSG. A cluster of three sources was found in a 10″ × 30″ area (objects 3, 4, and 5) at the position of VS-26, explaining the past confusion over its observation. The J, H, and K photometry of object 5 agrees well with colors presented for "VS-26" by Harris, Woolf, and Rieke (1978). 2 μm photometry of objects 13 and 15 by this study agrees well with that of Elias. It is difficult to compare our observations of objects 3, 4, and 5 and object 10 with those of VS-26 and object A by VSSG because of their 36″ beam size and the extended nature of these sources.

TABLE 1

POSITIONS AND PHOTOMETRY OF SOURCES DETECTED IN THE 2 MICRON SURVEY

Object Number	Previous Identification	$\alpha_{(1950)}$	$\delta_{(1950)}$	J	H	K	3.4 μm
7	...	$16^h23^m39^s.8$	−24°24′14″	...	13.71 ± 0.02	11.16, 10.86[a] ± 0.01	8.59[a] ± 0.09
8	...	16 23 40.3	−24 26 41	...	12.29 ± 0.03	9.42 ± 0.03	7.6 ± 0.2
12	...	16 23 42.5	−24 28 04	...	14.43[b] ± 0.04	11.02[b] ± 0.01	7.05[b] ± 0.02
2	...	16 23 46.8	−24 21 53	...	13.91 ± 0.03	10.96 ± 0.02	8.7 ± 0.1
18	...	16 23 47.4	−24 31 34	13.8 ± 0.1	11.50 ± 0.01	10.08 ± 0.01	8.6 ± 0.1
14	...	16 23 57.2	−24 29 08	...	13.29 ± 0.05	11.67 ± 0.02	9.2 ± 0.4
16	...	16 24 00.3	−24 30 44	13.97 ± 0.07	10.45 ± 0.01	7.82 ± 0.01	5.85 ± 0.01
1	...	16 24 01.9	−24 21 48	15.6 ± 0.4	12.98 ± 0.05	10.80 ± 0.03	9.1 ± 0.2
17	...	16 24 04.8	−24 31 33		13.8 ± 0.2	10.40 ± 0.01	7.91 ± 0.07
10	Object A (1)	16 24 07.3	−24 27 35	12.59 ± 0.09	10.19 ± 0.03	8.92 ± 0.03	7.9 ± 0.3
15	EL-29 (3)	16 24 07.8	−24 30 33	14.7 (3) ± 0.2	10.79 (3)	6.78 ± 0.01	3.88 (3)
9	...	16 24 09.3	−24 26 41	...	13.82[a] ± 0.06	11.89[a] ± 0.03	9.8[a] ± 0.5
11	...	16 24 09.5	−24 28 07	...	13.73[a] ± 0.04	11.71[a] ± 0.02	9.6[a] ± 0.4
19	...	16 24 09.7	−24 31 49	...	14.5[a] ± 0.1	10.71[a] ± 0.02	8.21[a] ± 0.07
20	...	16 24 13.9	−24 31 59	13.36[a] ± 0.08	10.74[a] ± 0.01	9.28[a] ± 0.01	8.12[a] ± 0.09
5	VS-26 (2)	16 24 16.4	−24 22 11	...	14.5 ± 0.1	10.29 ± 0.01	8.21 ± 0.06
4	VS-26 (1)	16 24 16.8	−24 22 23	14.4 ± 0.2	11.48 ± 0.01	9.63 ± 0.01	8.23 ± 0.06
3	...	16 24 17.6	−24 22 00	...	14.6 ± 0.1	11.34 ± 0.01	9.2 ± 0.1
6	...	16 24 19.8	−24 23 08	...	13.94 ± 0.02	9.93 ± 0.01	7.13 ± 0.01
13	VS-25 (1), EL-31 (3)	16 24 25.4	−24 24 34	12.36 (3)	10.43 (3)	9.30 ± 0.01	8.4 ± 0.1

NOTE.—Numbers in parentheses indicate references for previous identification and photometry. (1) Vrba *et al.* 1975. (2) Harris, Woolf, and Rieke 1978. (3) Elias 1978.

[a] Photometry was obtained with the 2.3 m telescope.

[b] Photometry was obtained using both the 1.54 m and 2.3 m telescopes.

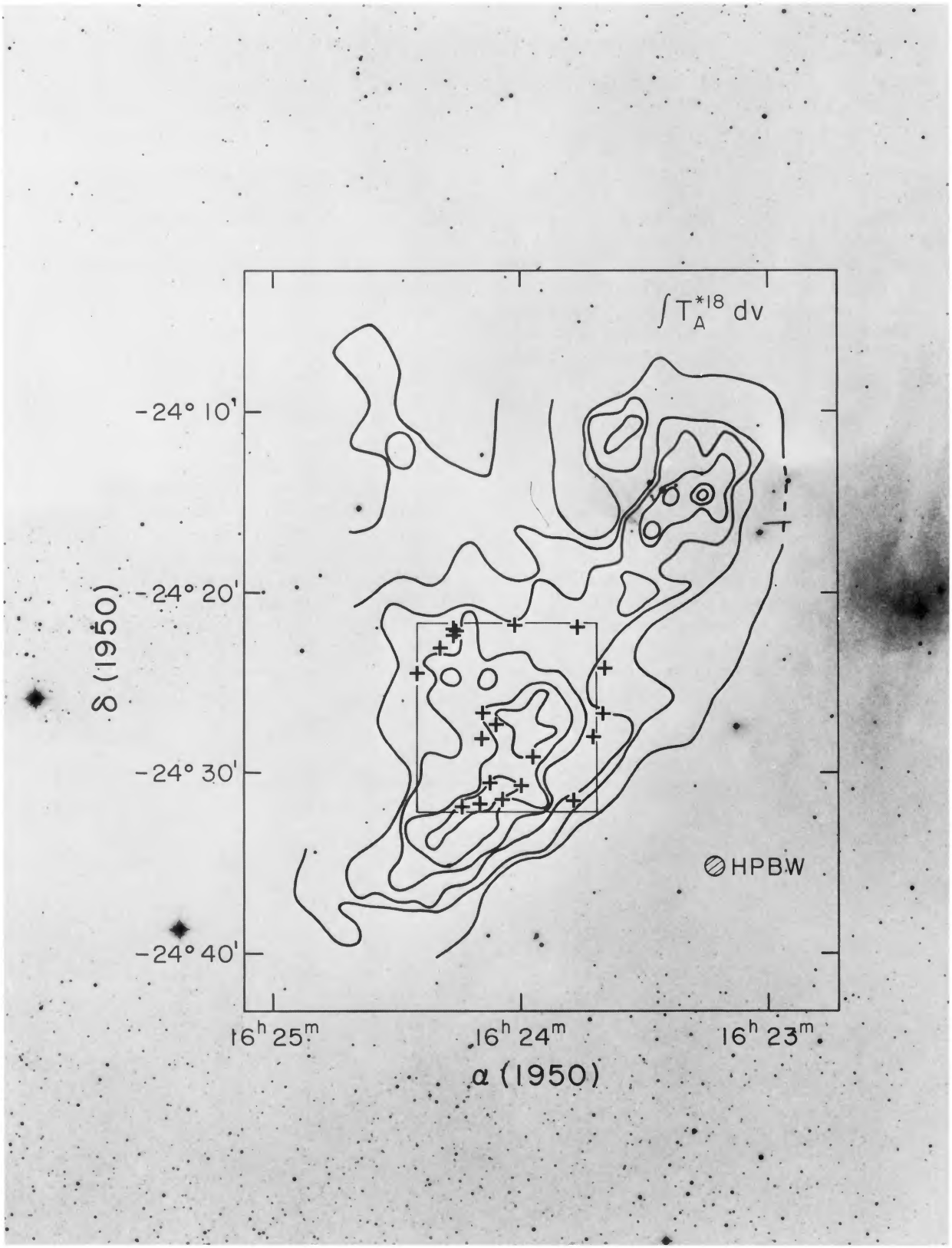

FIG. 2.—A map of $C^{18}O$ integrated intensity and the results of our 2 μm survey superposed on the red Palomar Sky Survey photograph of the ρ Oph dark cloud. Contours of $\int T_A^{*18}\,dv$ vary from 2 to 7 K km^{-1} s^{-1} in steps of 1 K km^{-1} s^{-1} as one goes from the outer to inner regions of the cloud. The 10′ × 10′.5 box encloses the area surveyed at 2 μm, and the 20 sources detected with $K < 12.0$ mag are denoted by a +. The bright reflection nebula to the west marks the position of HD 147889.

In addition to the 105 arcmin^2 box, a small area (3′ × 7.′7) north and west of source 1 was searched to a sensitivity of $K = 11.0$ in the same manner as described above. This survey concentrated on the highest extinction region of the northern core as defined by our $C^{18}O$ data. The 2 μm survey revealed no previously undetected sources. The survey was unable to confirm the existence of GS-33, GS-34, and VS-12.

Since our instantaneous 3:1 signal to *rms* noise was always better than 12.1 mag at K, and the instantaneous 3:1 signal to *peak-to-peak* noise varied from 11.6 to 12.0 mag at K, we conservatively estimate that our survey was complete to $K = +12.0$ mag with a 99% level of confidence. The fact that the number of sources detected increased linearly with magnitude between $K = 9$ and 12 mag is certainly consistent with our completeness estimate.

III. ANALYSIS AND RESULTS

A thorough analysis of the $C^{18}O$ data is undertaken to give us our first look at the gas and dust column density distributions in the central regions of the ρ Oph cloud. From these distributions, we can derive cloud masses and establish criteria to test the association of the 20 sources detected in our infrared survey with the cloud.

a) *The* $C^{18}O$ *Data: Column Densities and Mass of the Cloud*

i) *The Integrated Intensities*

The $C^{18}O$ emission in ρ Oph appears optically thin since, for the few positions which have also been observed in ^{13}CO, the $C^{18}O$ lines are considerably more symmetric and appear free of self-absorption (e.g., Fig. 1). Therefore, the determination of the $C^{18}O$ integrated intensity, as defined by $\int T_A^{*18}\, dv$, will give an unbiased estimate of the relative gas column density distribution across ρ Oph for a constant excitation temperature. A map of $C^{18}O$ integrated intensity in the Oph dark cloud is shown in Figure 2 superposed on the red Palomar Sky Survey photograph.

ii) $C^{18}O$ *Column Densities*

Without detailed knowledge of the temperature and density structure of the molecular gas, the determination of the column density of $C^{18}O$ gas must be made using a simplified cloud geometry. Adopting a LTE (local thermodynamic equilibrium) approach, the $C^{18}O$ column density is readily calculated assuming the emission arises from a homogeneous slab of gas. The self-absorbed profiles of ^{12}CO and ^{13}CO are evidence that the assumption of a constant excitation temperature along a column of gas in ρ Oph is not correct; a two-temperature slab model may be more appropriate. However, a two-temperature slab model based on the spike-pedestal structure of the $C^{18}O$ line presented in Figure 1 yields column densities within ~10% of those calculated for a single excitation temperature (Wilking 1981).

A complete derivation of the expression for the LTE $C^{18}O$ column density is presented in Wilking (1981) and yields the following:

$$N_{\rm LTE}^{18} = 2.42\times10^{14}(\tau_0\Delta v)(T_x + 0.89) \times \left[1 - \exp\left(5.27/T_x\right)\right]^{-1}, \quad (1)$$

where T_x is the gas excitation temperature, and τ_0 is the $C^{18}O$ line center optical depth. The quantity Δv is the full width at half-power of the $C^{18}O$ line in km s^{-1} and was determined by assuming Gaussian line shapes:

$$\Delta v = \int T_A^{*18}\, dv / T_A^{*18} pk. \quad (2)$$

The excitation temperature at each point was derived from the corresponding peak ^{12}CO $J = (1 \rightarrow 0)$ brightness temperature, T_B^{12}, obtained from the 62.5 kHz resolution map of T_A^{*12} presented by Loren *et al.* (1980). A forward beam coupling efficiency $\eta_f = 0.85$ was used to scale T_A^{*12} to T_B^{12} (Loren 1979). It should be noted that because of ^{12}CO self-absorption, these derived excitation temperatures will give only lower limits to the

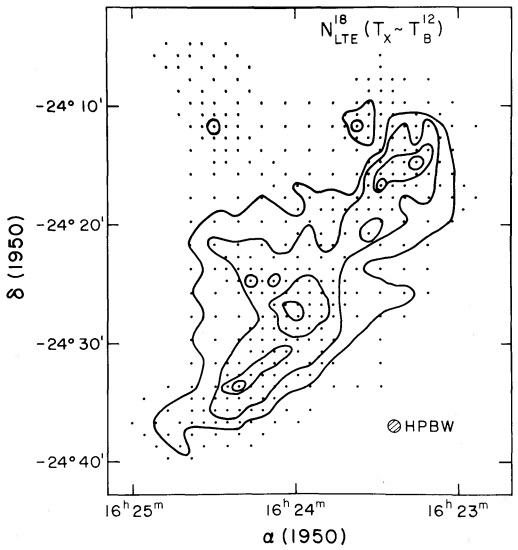

FIG. 3.—A map of LTE $C^{18}O$ column density (in units of 10^{16} cm^{-2}) in the central regions of the ρ Oph cloud. The contours of $N_{\rm LTE}^{18}$ increase from 1.0 to 2.5 toward the cloud center in steps of 0.5. The values of T_x were derived from the ^{12}CO brightness temperatures (ref. eq. [4]). In addition, the 360 points toward which $C^{18}O$ observations were made are shown.

true column density. The resulting map of $N^{18}_{\rm LTE}(T_x = T^{12}_B)$ is shown in Figure 3.

iii) *The Visual Extinction*

A convenient intermediate step toward obtaining the hydrogen column density and mass of the cloud involves computing the total visual extinction which corresponds to a given column of $C^{18}O$ molecules. This not only allows us to estimate the dust column density distribution in the cloud core but also gives us critical information with which to establish criteria to test the membership of our detected infrared sources with the cloud (§ III*b*). Final conversion to hydrogen column densities from A_v are made simply by assuming a gas-to-dust ratio.

The most straightforward method to convert our values of $N^{18}_{\rm LTE}$ to A_v involves the scaling of $N^{18}_{\rm LTE}$ to $N^{13}_{\rm LTE}$ and then the use of Dickman's (1978) empirical $A_v/N^{13}_{\rm LTE}$ relation. The above procedure and its implicit assumptions are discussed in detail in Wilking (1981) and yield

$$A_v/N^{18}_{\rm LTE} = 3.6\times10^{-15}\ \text{mag cm}^2. \qquad (3)$$

This relation is in close agreement with a similar ratio derived for both the ρ Oph and Taurus dark clouds by Frerking, Langer, and Wilson (1982).

A map of the visual extinctions which we estimate for the core region from our $C^{18}O$ column densities is shown in Figure 4. While the accuracy of these visual extinctions is subject to the 50% uncertainty of Dickman's relation, we have whenever possible taken the most conservative approach. Our assumed value for $N^{13}/N^{18} = 7$ is a lower limit (Wilking 1981) as are our values for $N^{18}_{\rm LTE}(T_x = T^{12}_B)$ owing to self-absorption. Therefore, we expect that more accurately determined values for A_v in ρ Oph will most likely increase these estimates.

iv) *Hydrogen Column Densities*

Mass estimates for the gas in the ρ Oph cloud can be obtained from hydrogen column densities, which can be most simply derived from our estimates for $N^{18}_{\rm LTE}$ and A_v by assuming an appropriate gas-to-dust ratio, $N_{\Sigma\rm H}/A_v$. The gas-to-dust ratio has been determined for the low-extinction ($A_v \sim 0$–2 mag) interstellar medium by Bohlin, Savage, and Drake (1978). Using ultraviolet data to measure hydrogen column densities toward 75 stars of known color excess, they obtain an average value of $N_{\Sigma\rm H}/E(B-V) = 5.8\times10^{21}$ cm^{-2} mag^{-1}, with an estimated error of only 6%. The theoretical justification for extending this gas-to-dust ratio to larger A_v has been discussed by Dickman (1978). There is insufficient evidence that the presence of large dust grains, as inferred by long wavelengths of maximum polarization and large values for $R = A_v/E(B-V)$, alters this ratio (see Wilking 1981). Dividing the average interstellar

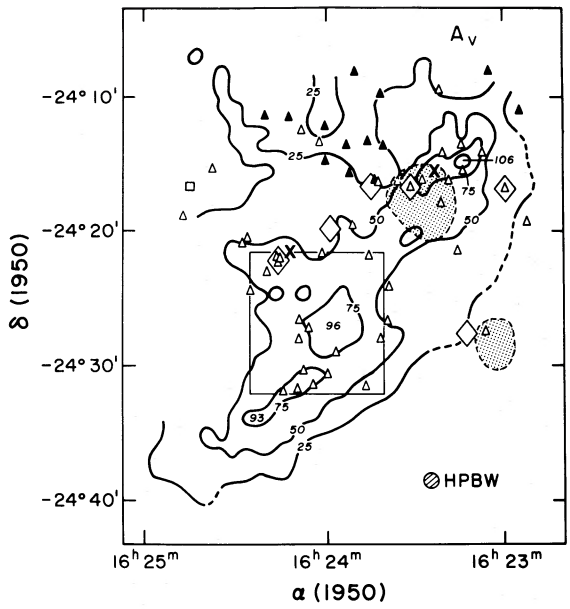

FIG. 4.—A map of visual extinction in the central core of the ρ Oph dark cloud as derived from our $C^{18}O$ data. Contours of A_v are marked in increments of 25 mag with the peak values given for the three largest enhancements. In addition to the 20 sources detected in our 2 μm survey, objects studied by other near-infrared surveys (GSS; VSSG; Elias 1978) are shown. Open triangles represent 42 of the 44 sources which have been determined to be embedded in the ρ Oph cloud by this study or by Elias (1978). Solid triangles denote sources which, at this time, cannot be classified as either members of the embedded cluster or background stars. The sole field star which has been identified in the central core, VS-13, is shown by an open square. Also displayed in this figure are (1) two of the 78 μm sources observed by Fazio *et al.* (1976), represented by dot patterns, (2) six sources of radio continuum radiation believed to be compact H II regions, indicated by large diamonds, as identified by Brown and Zuckerman (1975) or Falgarone and Gilmore (1981), and (3) two areas of high spatial density, marked by the *X*'s and characterized by strong SO emission (Gottlieb *et al.* 1978), 2 mm H_2CO emission, and rare 2 cm H_2CO emission at the easternmost position (Loren, Evans, and Knapp 1979; Loren *et al.* 1980).

$N_{\Sigma\rm H}/E(B-V)$ ratio by $R = 4$ yields

$$\frac{N_{\Sigma\rm H}}{A_v} = 1.4\times10^{21}\ \text{cm}^{-2}\ \text{mag}^{-1} \qquad (4)$$

for the ρ Oph cloud. This is consistent with the $N_{\Sigma\rm H}/A_v$ ratio of 1.9×10^{21} cm^{-2} mag^{-1} obtained by Whittet (1981) from an analysis of 12 stars in the ρ Oph dark cloud vicinity.

The cloud mass is finally determined by summing $N_{\Sigma\rm H}$, either observed or extrapolated, from each 1 arcmin^2 within the mapped area. Table 2 presents the masses derived for regions where $N^{18}_{\rm LTE}$ exceeds 2.1×10^{16} cm^{-2} ($A_v > 75$ mag), 1.4×10^{16} cm^{-2} ($A_v > 50$ mag), and 7×10^{15} cm^{-2} ($A_v > 25$ mag) (the 25 mag "contour" is bounded on the east by the edge of the map).

TABLE 2

CLOUD MASSES IN THE CORE REGION

Projected Area	$M/M_\odot$
$A_v > 75$ mag:	
North	20
Central	30
South	10
75 mag $> A_v >$ 50 mag	230
50 mag $> A_v >$ 25 mag	260
Total ($A_v > 25$ mag)	550

v) *Mass Distribution*

Our $C^{18}O$ map presents a picture of the ρ Oph dark cloud unlike any previous molecular-line map of the area (refer to Figs. 2–4 for the following discussion). A significant fraction of the mass of the ρ Oph cloud appears to be contained in a concentration of gas which is fairly compact and elongated along a northwest-southeast axis over an area of dimension $20' \times 40'$, or 1×2 pc. The western edge of this cloud core is sharply defined, while the eastern edges blend into lower density material. Along the ridge of this core of gas are three mass enhancements. The northernmost enhancement is also a region of high spatial density ($n[H_2] > 10^5$ cm^{-3}; marked by an *X* in Fig. 4) as determined from observations of SO (Gottlieb *et al.* 1978) and H_2CO (Loren, Sandqvist, and Wootten 1983). The central mass enhancement along the ridge is by far the largest in the cloud and is characterized by strong self-absorption in ^{13}CO emission lines (Lada and Wilking 1980; Wilking and Lada, unpublished data). Observations of H_2CO in this central region show that despite the high column densities, the area is not as heavily compressed and has spatial densities of about 10^4 cm^{-3} (Loren, Sandqvist, and Wootten 1983). The southernmost mass enhancement in the core region appears to continue the trend of decreasing spatial density along the ridge and a tendency for the gas to be more dispersed along the line of sight.

In addition to the northern mass enhancement seen in $C^{18}O$, another area of extremely high spatial density has been observed to lie on the eastern edge of the core region (also marked by an *X* in Fig. 4). This area displays strong SO emission (Gottlieb *et al.* 1978) as well as strong 2 mm and rare 2 cm H_2CO emission (Loren *et al.* 1980; Loren, Sandqvist, and Wootten 1983). The latter observations set a lower limit to the spatial density of $n(H_2) = 10^6$ cm^{-3}. This region must be very compressed since, as seen in Figure 4, it does not contribute significantly to the mass of the cloud.

The cloud masses derived from our $C^{18}O$ data are summarized in Table 2. For the entire area mapped in $C^{18}O$ we obtain a cloud mass of 550 $M_\odot$. Over one-half of this mass (290 $M_\odot$) is contained within the 50 mag contour shown in Figure 4, underlining the centrally condensed nature of the core region.

b) The Infrared Data: Identification of Embedded Objects

A detailed analysis of the infrared photometry presented in Table 1 is performed to gain insight into how many of the 20 objects found in our survey box are embedded in the ρ Oph dark cloud. Ideally, narrow-band photometry in and around the 2.3 μm CO band would be the simplest method to distinguish between embedded and background infrared stars (e.g., Elias 1978). Even with the high sensitivity of this survey, the high extinctions in our survey box (typically $A_v > 50$ mag) ensure that 95% of the background stars detected would be G (5%), or K or M giants (90%) (Elias 1978). Therefore, the majority of young stars which we would expect to observe embedded in ρ Oph should show no CO absorption at 2.3 μm. Unfortunately, only objects 6, 13, and 15 have been examined at 2.3 μm; object 6 by this study (no absorption), and objects 13 and 15 by Elias (possible absorption and no absorption, respectively).

With only broad-band photometry at our disposal, our task is not an easy one. In the following section, three separate arguments will be presented to show that all 20 sources are members of a population of young objects embedded in the ρ Oph dark cloud.

i) *Star Counts*

Counts of infrared sources in unobscured areas near ρ Oph have been performed by Elias (1978). With the 50 mag of extinction throughout our survey box, we have an effective limiting magnitude of less than 7.0 mag at 2.2 μm for the detection of background stars. Using Figure 4 from Elias's study, we estimate that less than one (0.4) background star is expected in our $10' \times 10'.5$ survey box at this sensitivity. On this statistical argument, the vast majority of objects detected in our survey would appear to be associated with the dark cloud.

ii) *Infrared Excesses*

With our broad-band photometry alone it may be possible to distinguish between stars associated with and background to the ρ Oph cloud by looking for evidence of an infrared excess at 3.4 μm (also referred to as *L*) in each object. Infrared excesses longward of 3 μm are common in young stars and arise from thermal radiation from a dust shell and/or free-free emission from a gaseous envelope surrounding and heated by the star (e.g., Cohen and Kuhi 1979). Infrared excesses in the 2–4 μm region are observed in some late *M* stars and carbon Mira variables (Merrill and Stein 1976), but these objects are not predicted to be a significant percentage of the background population. Therefore, ob-

jects which display infrared excesses are most likely young stars embedded in the ρ Oph cloud.

The presence of excess emission at 3.4 μm can be readily established by comparing the observed color excess ratio $E(K-L)/E(H-K)$ with the same ratio which is determined from the reddening alone. The reddening toward ρ Oph has been well studied by Elias (1978) from background stars which lie at the periphery of the dark cloud material. For the H to L spectral region, Elias finds

$$\frac{E(K-L)}{E(H-K)} = 0.56 \pm 0.04. \quad (5)$$

The observed values for $E(K-L)/E(H-K)$ are most simply formed from the raw colors presented in Table 1. Since the intrinsic $K-L$ and $H-K$ color indices are much smaller than the values which we observed (e.g., Frogel *et al.* 1978), $(K-L)/(H-K)$ is a very good approximation to the true color excess ratio. Therefore, our determination of possible 3.4 μm excess emission does not rely upon the knowledge of the underlying photospheric colors or of the distance.

Color excess ratios calculated for the 20 objects detected in our 2 μm survey are presented in the second column of Table 3. If the value for $(K-L)/(H-K)$ was found to exceed 0.60 (refer to eq. [5]) by more than its one sigma value (as calculated from the errors in the photometry), then the difference was attributed to excess emission at L. As a result, all but one of the infrared sources detected in our survey indicate excess emission at L and appear to be objects embedded in the ρ Oph cloud. Object 5 displays no excess emission at L.

TABLE 3

IDENTIFICATION OF EMBEDDED OBJECTS: INFRARED EXCESSES AND EXTINCTION

Object Number	$\frac{K-L}{H-K}$	L excess?	$A_v(H-K)$	$A_v(C^{18}O)$
1	0.79 ± 0.11	yes	25	50
2	0.76 ± 0.05	yes	35	51
3	0.67 ± 0.04	yes	38	57
4	0.76 ± 0.03	yes	21	54
5	0.49 ± 0.02	no	50	55
6	0.70 ± 0.01	yes	47	59
7	0.90 ± 0.04	yes	30	50
8	0.64 ± 0.02	yes	34	50
9	1.10 ± 0.28	yes	22	75
10	0.79 ± 0.07	yes	15	70
11	1.03 ± 0.19	yes	23	58
12	1.16 ± 0.02	yes	40	56
13	0.81 ± 0.09	yes	13	46
14	1.52 ± 0.26	yes	19	75
15	0.72 ± 0.01	yes	47	80
16	0.75 ± 0.01	yes	31	70
17	0.73 ± 0.04	yes	40	60
18	1.02 ± 0.09	yes	16	32
19	0.66 ± 0.03	yes	45	78
20	0.79 ± 0.06	yes	17	78

iii) *Extinction*

Utilizing our observed $H-K$ color indices and our estimates for A_v from the gas column densities, it may be possible to distinguish between associated and background infrared sources detected toward ρ Oph. From our observed $H-K$ colors, we can set an upper limit to the visual extinction toward each object independent of its distance. By assuming a star's intrinsic $H-K$ colors are zero, a visual extinction can be estimated toward the star which would only be reduced if one attempted to account for photospheric colors or circumstellar emission. By comparing this upper limit with the total cloud extinction toward each object, as derived from our $C^{18}O$ observations, we can determine whether the object must lie embedded in or background to the molecular cloud.

The maximum visual extinction toward a background star, $A_v(H-K)$, has been calculated given the $H-K$ colors for our 20 sources and $A_v \sim 12(H-K)$ (Elias 1978). These values are presented in the fourth column of Table 3. The total cloud extinction toward each object is entered as $A_v(C^{18}O)$ in the last column of Table 3. With the provision that these latter visual extinctions are representative of the total extinction through the ρ Oph cloud, and that there is no clumpiness within our 1'.1 beam of observation, then $A_v(C^{18}O)$ could never exceed $A_v(H-K)$ if the infrared sources were truly background. A comparison of these two estimates for the visual extinction leads us to the conclusion that most of the infrared sources detected in our survey are embedded in the cloud.

c) *Summary of Observational Results*

New and extensive millimeter-wave observations in ρ Oph have given us our first look at the gas column density distribution in the cloud (on an arc minute scale) and have allowed a more accurate determination of the cloud mass. Shown to be free of self-absorption and hence reliable tracers of cloud mass, $C^{18}O$ emission lines were observed toward 360 locations in the central regions of the cloud. Subsequent analysis of these data has revealed a 1×2 pc ridge within which lies the centrally condensed core of the ρ Oph cloud, where extremely large gas and dust column densities prevail: $N^{18}_{\rm LTE} = 1.4\text{–}2.9 \times 10^{16}$ cm^{-2} and $A_v = 50\text{–}106$ mag. A cloud mass of 550 $M_\odot$ is obtained for the area where $N^{18}_{\rm LTE}$ exceeds 7×10^{15} cm^{-2} ($A_v \geq 25$ mag).

Using our $C^{18}O$ observations as a guide, we have conducted a new and more sensitive 2 μm survey to a limiting magnitude of $K = +12.0$ mag of a 0.5×0.5 pc box centered on the region of highest extinction. This survey, which was 2 mag fainter than the deepest previ-

ous survey, has resulted in the detection of 20 (16 of which were heretofore undiscovered) infrared objects. Using our J, H, K, L photometry and our $C^{18}O$ data, we have demonstrated that probably all of the sources we detected are embedded within the cloud and are not background objects. This confirms earlier contentions that a dense population of young objects has recently formed within the ρ Oph cloud (GSS; VSSG; Elias 1978).

IV. THE NATURE OF THE EMBEDDED POPULATION IN THE CORE REGION

a) Size and Distribution

In addition to the 20 sources detected within our survey box, Figure 4 shows the numerous 2 μm sources detected throughout the core region by previous surveys. The entire area mapped in $C^{18}O$ was included in a search for 2 μm sources by Elias (1978) which had a limiting magnitude slightly brighter than $K = +8.0$ mag. Grasdalen, Strom, and Strom (GSS) have surveyed a portion of the core west of and including the northernmost mass enhancement to a sensitivity of $K = 9.0$ mag. Vrba *et al.* (VSSG) completed the GSS survey to a limiting magnitude of $K = 10.0$ mag to include most of the core region; their coverage is bounded in the south by the declination of the southern edge of our survey box.

Clearly not all of the 2 μm sources found in the four efforts to survey the core region of ρ Oph are embedded in the cloud. In our analysis of the sources detected in our survey (§ III*b*), we presented evidence that all 20 objects that we studied were associated with the cloud. On the basis of narrow-band photometry of the 2.3 μm CO band, Elias was able to assign 19 sources (including EL-29 = object 15) to a population of neo- or protostellar objects associated with the ρ Oph dark cloud. In addition to these 38 embedded stars, six objects (VS-1, GS-26, VS-4, VS-5, VS-21, and VS-27) can be included in this list because of their superposition on areas of high visual extinction (§ III*b*) and/or the orientation of their polarization position angles (Wilking *et al.* 1979). Hence, the number of objects thus far associated with the ρ Oph cloud totals 44, as listed in Table 4. Of these 44, 30 lie within the 50 mag contour, as shown in Figure 4.

In summary, our observations have led to a doubling in the number of objects known to be embedded in the ρ Oph cloud. Figure 4 shows the distribution of 42 of the 44 2 μm sources associated with the ρ Oph dark cloud. Denoted by open triangles, their distribution indicates that star formation has not been restricted to any particular area of the core region, and that the central core is not devoid of embedded stars as previous surveys had suggested. Not shown in Figure 4 are HD 147889 and SR-24, which are associated with the cloud and lie in areas of low extinction at the edges of the core region.

b) Luminosities: A Population of High- or Low-Mass Stars?

Critical to our understanding of the star formation process in ρ Oph is the form of the mass spectrum of the embedded population. In this section, we will estimate the mass of the 44 objects which we have determined to be members of the embedded population by combining our observations with those obtained by previous investigators at a variety of wavelengths. Reliable luminosity and mass estimates can be made for only seven of the 44 sources for which far-infrared, radio continuum, optical, as well as near-infrared, data exist. For the remaining 37 sources, somewhat cruder luminosity and mass estimates can be made from the analysis of their near-infrared colors alone.

i) *Far-Infrared, Radio Continuum, and Optical Data*

Completely sampled far-infrared (FIR) observations of the central regions of the ρ Oph cloud have been performed by Fazio *et al.* (1976). These observations had an effective wavelength of 78 μm (for a 50 K source temperature) and were sensitive to stars of spectral type B8–9 V and earlier which deliver all of their energy to the surrounding dust. Fazio *et al.* resolved only three FIR sources; extended FIR emission is observed around the B2 V star HD 147889 (optical classification by Garrison 1967) in addition to the two areas shown by the dot patterns in Figure 4. The southern source lies in an area of very hot CO emission ($T_A^* = 50$ K) and encompasses the star SR-3. The B6 V optical classification suggested for SR-3 (e.g., Elias 1978) is consistent with the presence of FIR emission. The northern FIR source shown in Figure 4 is the most highly peaked source and is excited by an early-type star designated as source 1 by VSSG (see also Harvey, Campbell, and Hoffmann 1979 for detailed FIR study of this source). Also associated with source 1 are a compact H II region (Brown and Zuckerman 1975) and an extensive C II and S II region (Pankonin and Walmsley 1978; Falgarone *et al.* 1978), leading to its classification of B3 ZAMS. Although selection effects could hinder the detection of some late B stars, the FIR observations indicate that these three early B stars are the most luminous members of the population of stars embedded in the ρ Oph core region.

As many as 10 of the 27 sources of radio continuum radiation which are observed toward the ρ Oph dark cloud have been identified as potential compact H II regions in the cloud by either Brown or Zuckerman (1975, BZ) or Falgarone and Gilmore (1981, FG). Of these 10, we will limit our discussion to the seven which

TABLE 4

CLUSTER MEMBERS IN THE CENTRAL CORE

OBJECT NAME[a]	VISIBLE STAR?[b]	ZAMS			LOW-LUMINOSITY PMS			ADOPTED PHOTOMETRY[d]
		Sp. Type	A_v	$L/L_\odot$[c]	Sp. Type	A_v	$L/L_\odot$	
HD 147889.....	yes	B2 V	4	5000	main sequence		5000	1
Source 1,[e]								
GS-35.....	yes	B3	12.5	1050	main sequence		1050	2, 3
SR-3,								
GS-25.....	yes	B6 V	6	500	main sequence		500	1
Do-Ar 24,[e]								
GS-28.....	yes	T Tauri star		3	late K	0	3	4
SR-4	yes	T Tauri star		5	K7	2	5	5
SR-9	yes	T Tauri star		4	K7	1	4	5
SR-24	yes	T Tauri star		4	K2	4	4	5
EL-29,[e]								
Obj. 15	no	B0	31	25000	...	10	109	2
Obj. 16[e]	no	B2	30	2900	...	0	4.5	6
Obj. 6[e]	no	B2	48	2900	...	0	3	6
Do-Ar 21,								
GS-23.....	yes	B3	8	1050	...	0	4	2, 4, 7
Obj. 5[e]	no	B3	50	1050	...	0	1.5	6
Source 2,[e]								
GS-32.....	yes	B3	18	1050	...	0	8	1, 3, 7
GS-30[e]	no	B3	29	1050	...	2.5	35	2
EL-24	yes	B3	15	1050	...	0	11	2
SR-21,								
VS-23	yes	B4	9	900	...	0	13	2, 7
VS-17[e].....	no	B4	29	900	...	0	4	1
Obj. 8[e]	no	B4	34	900	...	0	2	6
Do-Ar 24 E,[e]								
GS-31.....	yes	B4	9	900	...	0	2	1, 4
Obj. 17[e]	no	B5	41	790	...	0	1.5	6
Obj. 19[e]	no	B5	45	790	...	0	1.5	6
VS-14	yes	B5	10	790	...	0	4	2, 7
VS-1	no	B5	19	790	...	0	2	2, 7
GS-29[e]	yes	B6	14	500	...	0	3.5	2, 3, 7
GS-39	no	B6	21	500	...	0	1.5	2
GS-26[e]	no	B6	22	500	...	0	1.5	1
Obj. 12[e]	no	B7	41	300	...	0	3	6
Obj. 10[e]	no	B8	16	200	...	0	1	6
VS-27[e].....	no	B8	26	200	...	0	0.6	3
Obj. 2[e]	no	B9	35	120	...	0	0.5	6
Obj. 3[e]	no	B9	39	120	...	0	0.5	6
Obj. 4[e]	no	B9	22	120	...	0	0.7	6
Obj. 20[e]	no	B9	19	120	...	0	0.7	6
VS-18[e]	no	A0	22	80	...	0	0.7	1
Obj. 7[e]	no	A2	30	45	...	0	0.5	6
VS-25,								
Obj. 13	yes	A2	14	45	...	0	0.6	2, 6
VS-5[e]	no	A3	19	30	...	0	0.5	3
VS-21	yes	A5	13	20	...	0	0.8	3, 7
Obj. 1[e]	no	A7	26	10	...	0	0.5	6
Obj. 18	no	F2	16	5	...	0	0.5	6
VS-4[e]	no	F2	21	5	...	0	0.5?	3
Obj. 11[e]	no	G1	24	1	...	0	0.5	6
Obj. 9[e]	no	G4	23	1	...	0	0.5	6
Obj. 14[e]	no	G5	19	1	...	0	0.5	6

[a]Sources not designated as "Obj." have been previously identified by one or more of the following. Source, GS: GSS 1973. SR: Struve and Rudkjøbing 1949. Do-Ar: Dolidze and Arakeylyan 1959. VS: VSSG 1975. EL: Elias 1978.

[b]Optical identification from either red POSS plate or from Elias 1978 or Chini *et al.* 1977.

[c]Luminosities for early-type ZAMS stars were obtained from Panagia 1973 and all other stars from Allen 1973.

[d]References for photometry as follows: (1) Harris, Woolf, and Rieke 1978. (2) Elias 1978. (3) VSSG 1975. (4) Rydgren, Strom, and Strom 1976. (5) Cohen and Kuhi 1979. (6) This paper. (7) Chini *et al.* 1977.

[e]Infrared object is contained within the boundaries of the 50 mag extinction contour shown in Fig. 1.

lie in the core region. Except for BZ-3 (HD 147889), these potential compact regions are marked by open diamonds in Figure 4. Moving west to east are FG-10, FG-11, BZ-4, BZ-5, BZ-6, and FG-12.

The sensitivity of existing observations allows the detection of compact H II regions in the ρ Oph cloud excited by stars of spectral type B3 ZAMS and earlier. Hence, all of the compact H II regions in the core region would be expected to be detectable sources of FIR emission. But only BZ-3 and BZ-4 coincide with FIR sources discussed above and are consistent with excitation by a B2 star (HD 147889) and a B3 star (source 1), respectively. Both FG-10 and FG-12 appear coincident with near-infrared sources which display no apparent excess emission at 3.4 μm, Do-Ar 21 and object 5, respectively. BZ-5, BZ-6, and FG-11 are not clearly identified with near-infrared sources embedded in the cloud. The future identification of an embedded object with BZ-6 would confirm the high visual extinctions we have proposed for the core region. We interpret the failure to detect FIR emission toward five of these seven "potential" compact H II regions as evidence that these regions are not excited by massive B stars. It is possible that some of these radio continuum sources are either background sources or compact H II regions collisionally excited by early stellar winds from low-mass stars (Cohen, Bieging, and Schwartz 1982). However, further study of these sources is warranted before we can conclusively determine their nature. Nonetheless, from here forward, we will assume that there are only three early B stars conclusively identified within the cloud.

Optical data have assisted in the classification of the aforementioned three early B stars in the core region of the ρ Oph cloud. In addition, four stars in the core display optical spectra which have led to their classification as T Tauri stars (Rydgren, Strom, and Strom 1976; Cohen and Kuhi 1979; see Table 1). As a result, reliable luminosity and mass estimates exist for these seven objects. There are nine additional objects in the group of 44 embedded sources which have optical counterparts but which remain unclassified (Chini *et al.* 1977; Elias 1978; see Table 4).

ii) *Near-Infrared Data*

For the 37 objects which remain unclassified, very reliable mass estimates can be made using only infrared data if we assume that the observed infrared colors arise solely from the reddened photospheres of main-sequence stars. However, as pointed out in § III*b*, at least 19 of these embedded stars show evidence for circumstellar shells which may contribute a significant fraction of the emission observed in the near-infrared. Furthermore, stars with circumstellar dust and gas may not yet have evolved onto the main sequence. In this latter case, the determination of stellar masses is not a simple exercise. Since we cannot at the present time determine conclusively whether the embedded population is composed primarily of main-sequence or pre–main-sequence (PMS) stars, we will estimate the luminosities and masses of these 37 embedded stars for two extreme cases: (1) the embedded stars are ZAMS objects and their *JHK* colors arise from reddened photospheres, and (2) the stars are primarily low-luminosity PMS objects with circumstellar dust which contributes significant emission in the near-infrared. We will also present arguments which suggest that of these two alternatives, the second is most consistent with observations of ρ Oph made at all wavelengths.

A ZAMS population: an embedded cluster of early-type stars.—If we assume that the infrared emission observed at wavelengths from 1.25–2.2 μm arises from heavily reddened gaseous photospheres of ZAMS stars, we can precisely determine spectral types, luminosities, and masses for all of the embedded objects. This precise determination results because the intrinsic infrared color indices not only are insensitive to temperature for stars with surface temperatures greater than about 2000 K, but in addition, are typically very much smaller than the observed color indices toward the ρ Oph embedded sources. Consequently, extinctions are directly determined from the observed infrared color indices toward each object without any detailed knowledge of their intrinsic colors. Combining the extinction with the distance to ρ Oph (160 pc) allows one to ascertain accurately the absolute infrared magnitude of each source, which in turn uniquely determines their ZAMS spectral types, luminosities, and masses.

We have computed ZAMS spectral types and extinctions for the 37 embedded objects for which spectral types could not be determined from optical or FIR observations. The results are listed in Table 4. From this analysis, the population of young objects in the ρ Oph core region is comprised of 40 B0–G5 main-sequence stars with visual extinctions ranging from 4–50 mag and is heavily weighted toward early B stars. This population is similar to that suggested by VSSG following a similar analysis.

A low-luminosity population: an embedded cluster of PMS objects?—As pointed out by Fazio *et al.* (1976) and Elias (1978), a serious discrepancy exists between the number of early-type stars predicted by the above method (33) and the number actually observed through FIR observations (three). If on the ZAMS, the embedded objects would be capable of delivering as much as $5\times10^4\ L_\odot$ to the surrounding dark cloud material. This luminosity cannot be accounted for by existing FIR observations. It is clear that in the absence of extended FIR emission, most of the infrared sources in ρ Oph are lower luminosity objects ($M < 3.5\ M_\odot$) and do not represent an upper main-sequence population of embedded stars.

As discussed in § III*b*, 19 of the 20 objects detected in our survey show evidence for excess emission at 3.4 μm. Existing observations of seven of the 37 objects in the 5–20 μm spectral region indicate the presence of substantial mid-infrared luminosity and circumstellar dust (VSSG; Elias 1978; Harris, Woolf, and Rieke 1978). These observations raise the possibility that the observed near-infrared colors result from a combination of reddened photospheric and circumstellar dust and gas emission, and that these embedded stars have not yet evolved onto the main sequence.

Under such circumstances, obtaining mass estimates from infrared colors alone is a difficult task. In order to determine masses for the embedded stars, we first need to position them accurately on the H-R diagram and then adopt a set of pre–main-sequence evolutionary tracks in the event that the sources do not lie on the main sequence. To place a source on an H-R diagram requires knowledge of both its bolometric luminosity, $L_{\rm bol}$, and its effective temperature. Estimates of $L_{\rm bol}$ can be obtained from the broad-band near-infrared colors. Unfortunately, these observations offer no direct information concerning effective temperatures or spectral types.

Nonetheless, we can place useful limits on the masses of these 37 embedded stars from their bolometric luminosities. We have estimated $L_{\rm bol}$ for each object by fitting their observed colors with one- or two-temperature blackbody curves weighted by a $1/\lambda$ emissivity (such that $\tau = 1$ at 1 μm) and then numerically integrating the area enclosed by these curves. Because of our inability to calculate the reddening toward these objects and the scarcity of 5–20 μm data, two assumptions were made which may underestimate $L_{\rm bol}$. First, except for two objects, we integrated the energy distribution of each object without correcting their infrared colors for reddening by foreground extinction. It is not straightforward to estimate the extinction for objects with circumstellar shells using only broad-band near-infrared colors. For such sources, hot dust and gas shells could contribute significantly to the near-infrared emission. Excess emission at 2.2 μm would result in an overestimation of A_v from the $H - K$ color indices. In addition, we cannot be certain that the reddening law for circumstellar dust is the same as for the general interstellar cloud material. By not dereddening the energy distributions, we could underestimate $L_{\rm bol}$ unless the source photons absorbed at shorter wavelengths are recovered at longer wavelengths (typically 5–20 μm) within the beam of the photometric observations.

As a result of our inability to deredden the near-infrared colors for these objects, a second assumption was made, namely, that the peak flux for each source occurs at the maximum flux measured (typically 3.4 μm). Once again, this assumption will result in a lower limit to $L_{\rm bol}$ except for objects which have been observed at wavelengths near their peak emission. The 5–20 μm photometry which has been obtained for only a small sample of these objects demonstrates the importance of mid-infrared observations in defining the peak emission. Therefore, most of the bolometric luminosities which we calculate will be lower limits, their quality improving with the availability of mid-infrared observations.

The most accurately determined bolometric luminosities are those computed for the seven objects with 5–20 μm observations. Most of these objects have been observed near their peak emission, and their νF_ν energy distributions are falling off at 10 or 20 μm. For two objects which still radiate significant luminosity in the 10–20 μm region, we can roughly estimate their foreground extinction, and we dereddened their energy distributions. From the depth of their 9.7 μm silicate absorption features as observed by Elias (1978), and using $A_v/\tau_{9.7\,\mu{\rm m}} = 10$–20 (Rieke 1974; Gillett *et al.* 1975), we conservatively estimate $A_v = 10$ mag for EL-29 and $A_v = 2.5$ mag for GS-30. Our dereddening of the energy distributions of EL-29 and GS-30 coupled to our blackbody curve fits over all wavelengths helps to account for their luminosity longward of 20 μm.

The results of our calculations are shown in Table 4. A lower limit of 225 $L_\odot$ is obtained for the total luminosity of these 37 embedded objects. This is consistent with the observed absence of luminous FIR emission in the core region of ρ Oph. Combining these objects with the three early-type stars and four T Tauri stars in the core region yields a total stellar luminosity of 7×10^3 $L_\odot$ for the known embedded population in ρ Ophiuchi. Clearly, this total luminosity is dominated by the three early B stars. Not counting these B stars, the most luminous stars in this population are EL-29 (110 $L_\odot$) and GS-30 (35 $L_\odot$). Both of these objects have been discussed in detail by Elias and appear to be intrinsically cool protostars. Of the remaining objects, 19 have luminosities between 1 and 13 $L_\odot$, and 16 are less than 1 $L_\odot$.

As mentioned earlier, only limits to the masses of the 37 embedded objects can be obtained from their *true* bolometric luminosities if these objects have gaseous photospheres which are either (1) still contracting toward the main sequence and/or (2) obscured by circumstellar dust. We will assume that the presence of an optical counterpart indicates that an object has at least reached the convective-radiative phase of its PMS evolution (case 1). This criterion is supported by the double-peaked spectral energy distributions which are observed toward several of the visible stars in the ρ Oph core (e.g., SR-21, EL-24; Elias 1978) and which are characteristic of T Tauri stars. This double-peaked structure presumably arises from a reddened gaseous photosphere which peaks in the near-infrared and strong emission from circumstellar dust which peaks in the mid-infrared. As shown in Table 4, nine objects in our sample have

optical counterparts which we will interpret as indicating progress in their evolution to at least the convectlve-radiative phase.

The standard convective-radiative PMS tracks for the gaseous stellar photosphere (Iben 1965) approach the main sequence from either a higher or constant luminosity regime. Therefore, a PMS star on these tracks would possess an L_{bol} greater than or equal to its final ZAMS value. Hence we expect that for case 1 the true L_{bol} will provide a good upper limit to the star's mass. In fact, for $L_{bol} > 1\ L_{\odot}$, the true L_{bol} determines a well-defined range of mass (a factor of 2) which a star must possess if it is on a convective-radiative track.

To be conservative, we assume that the remaining stars which have no optical counterpart have gaseous photospheres which are obscured by circumstellar dust and may have yet to evolve to the top of their convective tracks (case 2). Little theoretical work has been done concerning evolutionary tracks for cool protostars which have yet to display emission from their gaseous photospheres. Model calculations by Stahler, Shu, and Taam (1980) for a 1 $M_{\odot}$ protostar suggest that in the early stages of core formation, the accretion of the core results in a very luminous dust photosphere whose luminosity exceeds that of the gas photosphere which first emerges at the top of its convective track (marking the end of core accretion). From this model, we will assume that for case 2 the evolution of a cool protostar from this high-luminosity regime to the convective track assures us that the point where its *true* L_{bol} intersects the main sequence sets an upper limit, albeit much cruder than the limit from case 1, to the star's ZAMS luminosity and hence mass.

The reliability of the masses derived for the 37 unclassified objects using the methods outlined above depends strongly upon our ability to calculate accurately the bolometric luminosity and to assess their evolutionary status. Thus, the most dependable mass estimates are for those embedded objects for which 5–20 μm photometry has been obtained and which are coincident with visible stars (and, in the most conservative case, are on the convective-radiative tracks of their pre–main-sequence evolution). Four objects, SR-21, EL-24, source 2, and GS-29, satisfy both of the above conditions, and their derived masses fall into the 1–2 $M_{\odot}$ range. Because they have no optical counterparts and yet have rather accurately determined bolometric luminosities, firm mass upper limits obtained for EL-29, GS-30, and VS-17 are less than 3.5 $M_{\odot}$ (A0 V), less than 2.5 $M_{\odot}$ (A3 V), and less than 1.5 $M_{\odot}$ (F2 V), respectively.

For the remaining 30 sources, our mass upper limits would suggest these objects are less massive than 1.5 $M_{\odot}$. However, there is no photometry for these objects longward of 3.4 μm and as a result we have probably underestimated their bolometric luminosities. However, since the mass of main-sequence stars is relatively insensitive to the luminosity, i.e., $M \propto L^{(1/3.5)\rightarrow(1/4)}$, these rough guesses for the mass estimates will be good to a factor of 2 if the luminosities are not underestimated by more than a factor of ~ 15.

In summary, based upon the FIR observation of Fazio *et al.*, we have treated the 37 unclassified objects as a population of low-luminosity stars with circumstellar dust and gas. This conjecture is supported by the infrared excesses found for the vast majority of objects with 3.4–20 μm photometry. Our estimation of their bolometric luminosities gives a lower limit to the total luminosity available from these objects which is consistent with the failure to detect luminous far-infrared emission toward ρ Oph. For the seven objects for which we could reliably determine mass limits from L_{bol}, most appear to fall in the 1–2 $M_{\odot}$ range except for EL-29 and GS-30, which could form slightly more massive stars. With the provision that we have not grossly underestimated L_{bol} for these objects, mass upper limits for these and the remaining objects are consistent with the FIR observations and the absence of any objects more massive than 3.5 $M_{\odot}$, with the exception of three early B stars. However, additional 5–20 μm photometry of these objects is necessary before we can discuss the distribution of mass and ages of such a low-luminosity population.

V. STAR FORMATION IN THE ρ OPH CORE REGION

a) The Star Formation Efficiency

We are interested in determining whether or not star formation in ρ Oph will result in the production of a bound cluster. The formation of bound stellar systems is an important problem since star formation in molecular clouds often leads to rapid disruption and dispersal of star-forming gas (e.g., Elmegreen and Lada 1977; Whitworth 1979). In order for bound stellar systems to form, a considerable fraction of the original gaseous binding mass of the cloud must be converted into stars before the gas is dispersed. Otherwise, an unbound stellar group will result (Duerr, Imhoff, and Lada 1982).

How much mass needs to be processed into stars in order to ensure that a bound cluster is formed? If the cluster-forming cloud of mass M_i and radius R_i is initially bound and in virial equilibrium with a velocity dispersion V_i, then the virial theorem requires

$$M_i V_i^2 = G M_i^2 / R_i , \tag{6}$$

or

$$V_i = \sqrt{G M_i / R_i} . \tag{7}$$

After some time, a fraction of the original gaseous mass,

f, will be processed into stars such that $f = M_\star/M_i$. This new system, consisting of both stars and gas, will still remain bound, and as a first approximation, both stars and gas will have a velocity dispersion given by eq. (7). Now, if the unprocessed gas is suddenly removed from the system by such dynamic forces as stellar winds, H II regions, or supernovae, only the stars will remain. The escape velocity for this bare stellar system is simply

$$V_{\rm esc} = \sqrt{2GM_\star/R_i}\,. \tag{8}$$

In order for this stellar system to remain bound requires $V_i < V_{\rm esc}$, or combining eqs. (7) and (8),

$$\frac{M_\star}{M_i} > 0.5.$$

Therefore, at least 50% of the original binding mass must be converted into stars to produce a bound stellar group. If gas is removed slowly from the system, an efficiency of slightly less than 50% could produce a bound cluster. However, since rapid gas dispersal is suggested from observations of molecular clouds, we will assume that a bound cluster will result only if roughly 50% of its original binding mass is processed into stars before dispersal.

In order to determine whether the stellar system in ρ Oph will ultimately become a bound cluster, we will combine our knowledge of the gaseous and stellar mass in ρ Oph to calculate the star formation efficiency (SFE). We define the star formation efficiency as

$$\text{SFE} = f = \frac{M_\star}{M_\star + M_{\rm gas}}\,. \tag{9}$$

If SFE $\gtrsim 0.5$, a bound cluster will ultimately emerge.

A meaningful SFE is obtained only when the mass of gas is determined for that volume occupied by the embedded stars. To calculate the SFE in ρ Oph, we consider only the stars and gas in a layer which is enclosed by the 50 mag extinction contour in the central core region (see Fig. 4) and whose depth is defined by the maximum extinction estimated for the embedded objects. Except for a small section south of our survey box, most of the area enclosed by the 50 mag contour has been surveyed at 2 μm to either $K = +10$ mag (38%) or $K = +12$ (48%). Without resolving the dilemma of the nature of the embedded sources, we shall calculate the star formation efficiency for two cases: (1) the embedded sources are main-sequence objects, except for one T Tauri star, and (2) the embedded sources are low-luminosity objects, except for source 1. These two cases will provide an upper and lower limit to the true SFE. The results of the following discussion are summarized in Table 5.

i) *Early Main-Sequence SFE*

There are 30 cluster members which are contained within the 50 mag extinction contour. If their near-infrared colors are composed of only reddened photospheric emission, then these objects (excluding one T Tauri star) would possess ZAMS spectral types ranging from B0 to G5 and visual extinctions ranging from 8 to 50 mag (see Table 4). An observed total stellar mass of 164 $M_\odot$ is computed for these 30 cluster members. The maximum extinction to which we can view these objects (50 mag) defines a layer for which the mass of gas can be calculated. Adopting a gas-to-dust ratio of $N_{\Sigma\rm H}/A_v = 1.4\times10^{21}$ cm^{-2} mag^{-1} (see eq. [4]) and using the projected area of the 50 mag extinction contour (0.4 pc) yields $M_{\rm gas} = 227\ M_\odot$. This results in a raw SFE of 42%.

For a more realistic estimate of the star formation efficiency of ZAMS objects, we can account for cluster members which would be hidden by extinction in this 50 mag layer. By calculating the maximum depth into this layer to which each 2 μm survey was capable of penetrating for each absolute magnitude interval, we can correct the observed number of sources assuming a constant density of sources per extinction. Thus, the true number of stars N in an absolute magnitude interval M_K which lie in a layer of gas and dust to a depth $\tau_c = 50$

TABLE 5

STAR FORMATION EFFICIENCIES AND STELLAR DENSITIES

Embedded Population within 50 mag Contour	($M/M_\odot$) Stars	SFE (%)	$M_\odot$ pc^{-3}
ZAMS (except for one T Tauri star)			
Observed	164	41	330
Corrected for extinction	199	47	400
Low-luminosity PMS (except for source 1)			
Observed	38	28	190
Corrected for extinction and nonuniform limits of detection	51	34	250

mag is given by

$$N_{\rm true}(M_K) = 0.1\tau_c/(m_l - M_K - {\rm DM})\,N_{\rm obs}(M_K), \quad (10)$$

where m_l is the limiting K-magnitude to which the area of interest has been surveyed, and DM is the distance modulus for the ρ Oph cloud (6 mag). Clearly, our determination of each star's absolute magnitude relies upon its identification as a ZAMS object.

The total mass of ZAMS stars which are predicted to lie in the 50 mag layer is 199 $M_\odot$. This implies an actual SFE of 47%. This value could be raised even further if we accounted for the unsurveyed area of the central core (14% of the total) and corrected for the lower mass ZAMS members which were too faint to be detected.

ii) *Low-Luminosity SFE*

The possibility has been raised that the embedded population in ρ Oph is comprised of primarily low-luminosity objects with circumstellar dust. Based upon the limited information available to us concerning the bolometric luminosities of these objects, a lower limit to the SFE would be provided if we characterize 29 of the 30 objects which lie within the 50 mag contour by an average mass of 1 $M_\odot$. Assuming there is no excess emission at 2.2 μm and assuming each star has at least reached the convective track of its pre–main-sequence evolution, a 1 $M_\odot$ star will have the luminosity of a main-sequence G5 star ($M_K = 3.7$ mag). Therefore, the total observed stellar mass is 38 $M_\odot$ with source 1 included as a 9 $M_\odot$ object.

Because we have characterized this population by a single absolute magnitude, the maximum depth to which our survey was able to detect these objects would be 22 mag. The mass of gas contained in a 22 mag layer whose projected area is equal to that of the 50 mag extinction contour is 100 $M_\odot$. This results in a raw SFE of 28% for this layer.

A more accurate estimate of the SFE is obtained if we can include those members of the low-luminosity population which are either (1) hidden by extinction in a 22 mag layer in areas which were surveyed to only $K = +10$ or (2) in areas which were not surveyed. Consideration of these two factors adds about 13 objects to the population of stars in the outer 22 mag of the cloud. This revised total stellar mass is 51 $M_\odot$, and the SFE is 34%. This SFE could be increased if some members are found to be main-sequence stars, or if we tried to account for objects less luminous than our limits of detection.

b) Stellar Densities and Total Stellar Content

The mass in stars per cubic parsec within the central core of the ρ Oph cloud can be computed for direct comparisons with stellar densities found in other stellar aggregates such as open clusters, T associations, and young star-forming areas. Not only is the stellar density an indicator of youth and the intimacy of the embedded population with its surrounding dark cloud material, but it also gives a measure of the stability of the stellar group against disruption by galactic tides and passing interstellar clouds (Bok 1934; Spitzer 1958).

Stellar densities in ρ Oph have been computed by utilizing the same assumptions for the nature of the embedded population within the 50 mag extinction contour as in the previous section and by calculating the volume which they occupy. This volume can be approximated by the volume of uniform density gas in a plane-parallel slab, given an appropriate spatial density. Observations of H_2CO by Loren, Sandqvist, and Wootten (1983) indicate that $n(H_2)$ exceeds 10^4 cm^{-3} over most of the central core region. This results in a volume of 0.5 pc^3 for a 50 mag layer and 0.2 pc^3 for a 22 mag layer assuming that 10^4 cm^{-3} is the average spatial density in the total column of gas. The stellar densities determined for the central core of ρ Oph are summarized in Table 5.

By calculating the SFE and stellar density in a well-defined layer coexistent with the embedded population, we have avoided the uncertainties introduced when deriving masses from CO emission lines. Instead, we depend on the more accurately determined gas-to-dust ratio. Nevertheless, we have relied upon our millimeter-wave observations to define, in a relative sense, the regions of high extinction which form the central core of ρ Oph. In addition, the large values which we have conservatively derived for the total extinction in the core from our $C^{18}O$ data (§ III*a* or Fig. 4) indicate that our use of these star-forming layers is reasonable in the sense that their depth does not exceed the actual extent of the cloud.

The determination of the total stellar content in the ρ Oph cloud requires us to adopt a cloud geometry which is directly based upon the masses and extinctions derived from our $C^{18}O$ data. Our estimate of 290 $M_\odot$ for the gas contained within the 50 mag extinction contour suggests that the central core can be characterized by an average total visual opacity of $\tau_c = 66$ mag. Following the procedure outlined in § V*a*, we can estimate the size of the embedded population which is hidden by extinctions greater than those of the 50 or 22 mag layers which we have considered in the previous sections and which do not exceed 66 mag. As a result, we obtain 135 $M_\odot$ (126 objects) and 240 $M_\odot$ (60 objects) for the total stellar mass of the ρ Oph cluster if the cluster members are primarily low-luminosity and early-type ZAMS stars, respectively. These total masses for the ρ Oph cluster contained in only a 0.4 pc^2 area are not unlike those observed for entire open cluster systems such as the Pleiades (416 $M_\odot$; Jones 1970), the Hyades (300 $M_\odot$; Pels, Oort, and Pels-Kluyver 1975), and IC 5146 (240 $M_\odot$; Walker 1959).

c) *Implications*

i) *The Formation of a Bound Cluster in ρ Oph*

Whether we regard the population of embedded objects as ZAMS or low-luminosity PMS in nature, the star formation efficiency in the central core of the ρ Oph cloud is very high: 34%–47%. This value for the SFE is 3–5 times greater than the largest efficiencies estimated for T associations under the same assumptions (Cohen and Kuhi 1979). Most recently, the SFE in the λ Ori T association has been computed to be only 0.2%–0.3% (Duerr, Imhoff, and Lada 1982).

In the absence of disruptive forces, it is very likely that the molecular gas in ρ Oph will continue to process gas into stars and raise the SFE to a number which exceeds 50%. At the present time, there is no evidence for forces within the molecular cloud capable of dispersing the cloud. This is supported by the narrow molecular lines and small velocity dispersions for the gas ($\Delta v \sim 1$–3 km s^{-1}) observed toward ρ Oph, which are characteristic of quiescent star-forming areas. The extremely high stellar densities which we calculate for the central core region, 250–400 $M_\odot$ pc^{-3}, are a factor of 10–100 times greater than those found in open clusters and T associations (Cohen and Kuhi 1979) and comparable only to densities estimated for two other regions which are sites of young star-forming activity: IC 348 (Blaauw 1964; Strom, Strom, and Carrasco 1974) and the Orion Trapezium cluster (e.g., Herbig 1982). These high stellar densities reflect the high degree of stability which the stars in ρ Oph have against external disruptive forces such as galactic tides and passing interstellar clouds. Therefore, it is our conclusion that the star formation process in the ρ Oph cloud will proceed undisturbed and will ultimately result in a *bound* cluster.

The observed absence of luminous far-infrared emission from the central core, the low velocity dispersions of the molecular gas, and the evidence for circumstellar dust for most of the embedded stars argue strongly for a cluster composed primarily of low-luminosity pre–main-sequence stars rather than a cluster of early-type ZAMS stars. A cluster dominated by low-luminosity objects is further supported by reliable mass estimates for 11 of the cluster members; four T Tauri stars with masses in the 1–5 $M_\odot$ range (Cohen and Kuhi 1979) and seven objects which we have determined are less than 3.5 $M_\odot$. Furthermore, unless we have seriously underestimated their bolometric luminosities, 30 of the remaining 33 cluster members also appear to be low-luminosity objects with masses less than 1.5 $M_\odot$.

However, we note that it is possible that we have underestimated the luminosities and masses of at least some stars in this latter group since we did not correct for reddening in determining their luminosities. The fact that those objects whose $(H-K)$ color indices exceed ~1.7 have no optical counterparts suggests that many objects are deeply embedded in the cloud, and a proper accounting for reddening could significantly increase the luminosity estimates for at least some sources. Unfortunately, accurate extinction estimates cannot be made for most of these objects. However, since we expect that most of the luminosity absorbed at near-infrared wavelengths will be reradiated at longer wavelengths, additional 5–20 μm observations of the embedded stars should result in considerably more reliable luminosity and mass estimates than are available now. Nonetheless, for the majority of objects, we have probably underestimated the luminosities by no more than a factor of 10 and the masses by no more than a factor of 2.

As discussed earlier, the most massive members of the cluster are HD 147889 (B2), source 1 (B3), and SR-3 (B6), which are the only sources that can be conclusively identified as B stars on the basis of far-infrared and radio continuum data. In addition, there are two other infrared objects which are not far-infrared sources but are associated with radio continuum sources: Do-Ar 21 and object 5. These objects may well be more luminous and massive than we have estimated, and 5–20 μm photometry is necessary to determine whether in fact this is the case. Based on the above discussion, we conclude that the embedded cluster in ρ Oph is composed primarily of low-luminosity, pre–main-sequence stars and is not a cluster of luminous, early-type ZAMS objects. Additional 5–20 μm observations of the embedded objects and/or better far-infrared (e.g., 100–350 μm) data would help to make this conclusion more firm.

Finally, it is interesting to speculate how the star formation process in ρ Oph has produced such a high SFE compared with other star-forming regions. Either stars have formed continuously at a similar rate as in other regions, but over a much longer period of time, or they have formed in a much more rapid and efficient burst of activity. There is evidence that stars can form continuously in bound open clusters over long periods of time. For example, in the Pleiades, the discrepancy between the nuclear and contraction age derived for the cluster implies that low-mass stars were forming as much as 175 million years before high-mass stars formed (Herbig 1962; Landolt 1979; Stauffer 1980). The suggested preponderance of pre–main-sequence objects in the ρ Oph cluster, however, would seem to suggest an efficient and rapid formation episode for this cluster. without better knowledge of the luminosities, masses, and evolutionary states of the embedded objects in ρ Oph, we cannot conclusively determine the duration of star formation in the ρ Oph cloud. However, additional 5–20 μm photometry may make possible such a determination.

Ultimately, it must be the physical condition of the molecular material which determines how rapidly and efficiently gas is processed into stars. Although we cannot say precisely what the requisite cloud properties are

that produce a bound cluster, there are several distinct properties of the ρ Oph cloud which set it apart from OB and T association–forming complexes. Unlike OB complexes, the velocity dispersions in the molecular gas of ρ Oph are low and characteristic of clouds forming low-mass stars. In contrast to OB and T association complexes, the ρ Oph cloud is much more centrally condensed with a significant fraction (as much as 50%) of its mass concentrated in a 1×2 pc core which occupies about 1% of the projected area of the ρ Oph complex. Extensive areas within the core region display spatial densities of 10^4–10^6 cm^{-3}. Giant molecular clouds often contain similar dense fragments of comparable or greater mass, but these fragments usually contain a much smaller fraction ($<10\%$) of the total cloud mass (e.g., M17 SW, W3, Orion KL, S252, NGC 1333). What relation these conditions have to the formation of a bound cluster is unclear at this time. However, further analysis of molecular observations of ρ Oph and comparison with other active clouds should improve our understanding of the formation of bound and unbound stellar groups from molecular clouds.

VI. CONCLUSIONS

New millimeter-wave and near-infrared observations in the ρ Oph dark cloud have been performed to obtain the data base necessary to determine if the star formation process in ρ Oph will produce a bound cluster. We have shown that at the time of the dispersal of gas from a young embedded cluster of stars, at least 50% of the initial cloud mass must have been converted into stars if the cluster is to remain bound. A synthesis of our new data with existing infrared, radio, and optical data permits us to calculate the star formation efficiency in the central regions of the ρ Oph cloud and to investigate the detailed star formation process in this region. The results of our study are summarized below:

1. Our $C^{18}O$ observations of the central regions of the cloud have revealed a 1×2 pc ridge of extremely large gas column densities within which lies the centrally condensed core of the ρ Oph cloud. Gas and dust column densities in the core are in the range $N^{18}_{\rm LTE} = 1.4$–2.9×10^{16} cm^{-2} and $A_v = 50$–106 mag. A cloud mass of 550 $M_\odot$ is obtained for the area where $N^{18}_{\rm LTE}$ exceeds 7×10^{15} cm^{-2} ($A_v \geq 25$. mag).

2. Our 2 μm survey of a 105 arcmin^2 region of highest extinction has resulted in the detection of 20 infrared objects (16 of which were heretofore undiscovered) in an area once thought to be devoid of such objects. Using our $C^{18}O$ data and near-infrared photometry, we have demonstrated that probably all of the sources we detected are embedded in the cloud.

3. Combining our new data with existing near-infrared studies has led to the identification of 44 infrared sources embedded in the central regions of ρ Oph. This represents more than a doubling of the previously known embedded population.

4. From two extreme assumptions as to the nature of the embedded population, i.e., low-luminosity or early-type ZAMS stars, we have computed the star formation efficiency in the central core. Regardless of our initial assumptions for the stellar masses, the resulting SFE is quite high: 34%–47%. With the observed absence of disruptive forces within the cloud, the formation of a bound cluster in ρ Oph appears imminent.

5. The observed absence of luminous far-infrared emission from the central core, the low velocity dispersions in the molecular gas, and evidence for circumstellar dust for many of the embedded sources strongly suggest that, with the exception of three early B stars, the embedded population in ρ Oph is comprised primarily of low-luminosity stars which may still be contracting toward the main sequence. By computing their bolometric luminosities, we have obtained mass estimates for these objects and showed they could be characterized as stars in the 1–3.5 $M_\odot$ range. However, additional mid-infrared observations of these objects are necessary to confirm this proposed dominance of low-luminosity objects.

First and foremost, we would like to thank George Rieke and Marcia Lebofsky for their encouragement throughout this study and their invaluable advice on the infrared observations. Inspiration and encouragement were also provided by Bart J. Bok. For assistance with the observations, we thank Marc Kutner, Frank Taylor, Kevin Housen, and John Weaver, with a special thanks to Elizabeth Stobie for her invaluable assistance with our millimeter-wave reduction. It is our pleasure gratefully to acknowledge Bob Loren, Al Wootten, Phil Meyers, Richard Crutcher, Steve and Karen Strom, Marc Adams, Bruce Elmegreen, and Bill Gilmore for many worthwhile discussions. Finally, we thank Ginette Hickman for the typing of this manuscript. This research was supported, in part, by the National Science Foundation.

REFERENCES

Allen, C. W. 1973, *Astrophysical Quantities* (3d ed.; London: Athlone Press).
Bertiaud, F. C. 1958, *Ap. J.*, **128**, 533.
Blaauw, A. 1964, *Ann. Rev. Astr. Ap.*, **2**, 213.
Bohlin, R. C., Savage, B. D., and Drake, J. F. 1978, *Ap. J.*, **224**, 132.
Bok, B. J. 1934, *Harvard Circ.*, No. 384.
Bok, B. J. 1956, *A.J.*, **61**, 309.
Brown, R. L., and Zuckerman, B. 1975, *Ap. J.* (*Letters*), **202**, L125.
Chini, R., Elsasser, H., Hefele, H., and Weinberger, R. 1977, *Astr. Ap.*, **56**, 323.
Cohen, M., Bieging, J. H., and Schwartz, R. D. 1982, *Ap. J.*, **253**, 707.
Cohen, M., and Kuhi, L. V. 1979, *Ap. J. Suppl.*, **41**, 743.

Dickman, R. L. 1978, *Ap. J. Suppl.*, **37**, 407.
Dolidze, M. V., and Arakeylyan, M. A. 1959, *Soviet Astr.—AJ*, **3**, 434.
Duerr, R., Imhoff, C., and Lada, C. J. 1982, *Ap. J.*, **261**, 135.
Elias, J. H. 1978, *Ap. J.*, **224**, 453.
Elmegreen, B. G., and Lada, C. J. 1977, *Ap. J.*, **214**, 725.
Falgarone, E., Cesarsky, D. A., Encrenaz, P. J., and Lucas, R. 1978, *Astr. Ap.*, **65**, L13.
Falgarone, E., and Gilmore, W. 1981, *Astr. Ap.*, **95**, 32.
Fazio, G. G., Wright, E. L., Zelik, M., III, and Low, F. J. 1976, *Ap. J. (Letters)*, **206**, L165.
Frerking, M. A., Langer, W. D., and Wilson, R. W. 1982, *Ap. J.*, **262**, 590.
Frogel, J. A., Persson, S. E., Aaronson, M., and Matthews, K. 1978, *Ap. J.*, **220**, 75.
Garrison, R. F. 1967, *Ap. J.*, **147**, 1003.
Gillett, F. C., Forrest, W. J., Merrill, K. M., Capps, R. W., and Soifer, B. T. 1975, *Ap. J.*, **200**, 609.
Gottlieb, C. A., Gottlieb, E. W., Litvak, M. M., Ball, J. A., and Penfield, H. 1978, *Ap. J.*, **219**, 77.
Grasdalen, G. L., Strom, K., and Strom, S. E. 1973, *Ap. J. (Letters)*, **184**, L53 (GSS).
Harris, D. H., Woolf, N. J., and Rieke, G. H. 1978, *Ap. J.*, **226**, 829.
Harvey, P. M., Campbell, M. F., and Hoffmann, W. F. 1979, *Ap. J.*, **228**, 445.
Herbig, G. H. 1962, *Ap. J.*, **135**, 736.
_____. 1982, in *Symposium on the Orion Nebula to Honor Henry Draper*, ed. A. E. Glassgold, P. J. Huggins, and E. L. Schucking (*Ann. NY Acad. Sci.*, Vol. **395**), p. 64.
Hills, J. G. 1980, *Ap. J.*, **235**, 986.
Iben, I., Jr. 1965, *Ap. J.*, **141**, 993.
Jones, B. F. 1970, *A. J.*, **75**, 563.
Lada, C. J. 1976, *Ap. J. Suppl.*, **32**, 603.
Lada, C. J., and Wilking, B. A. 1980, *Ap. J.*, **238**, 620.
Landolt, A. U. 1979, *Ap. J.*, **231**, 468.
Loren, R. B. 1979, personal communication.
Loren, R. B., Evans, N. J., II, and Knapp, G. R. 1979, *Ap. J.*, **234**, 932.
Loren, R. B., Sandqvist, Aa., and Wootten, A. 1983, *Ap. J.*, **270**, 620.
Loren, R. B., Wootten, A., Sandqvist, Aa., and Bernes, C. 1980, *Ap. J. (Letters)*, **240**, L165.
Low, F. J., and Rieke, G. H. 1974, in *Methods in Experimental Physics*, ed. N. Carleton (New York: Academic Press), p. 415.
Mermilloid, J. C. 1980, in *IAU Symposium 85, Star Clusters*, ed. J. E. Hesser (Dordrecht: Reidel), p. 129.
Merrill, K. M., and Stein, W. A. 1976, *Pub. A.S.P.*, **88**, 285.
Myers, P. C., Ho, P. T. P., Schneps, M. H., Chin, G., Pankonin, V., and Winnberg, A. 1978, *Ap. J.*, **220**, 864.
Panagia, N. 1973, *A.J.*, **75**, 929.
Pankonin, V., and Walmsley, C. M. 1978, *Astr. Ap.*, **64**, 333.
Pels, G., Oort, J. H., and Pels-Kluyver, H. A. 1975, *Astr. Ap.*, **43**, 423.
Rieke, G. H. 1974, *Ap. J. (Letters)*, **193**, L81.
Rieke, G. H., Montgomery, E. F., Lebofsky, M. J., and Eisenhardt, P. R. 1981, *Appl. Optics*, **20**, 814.
Roberts, M. 1957, *Pub. A.S.P.*, **69**, 59.
Rydgren, A. E., Strom, S. E., and Strom, K. M. 1976, *Ap. J. Suppl.*, **30**, 307.
Spitzer, L. 1958, *Ap. J.*, **127**, 17.
Stahler, W. S., Shu, F. H., and Taam, R. E. 1980, *Ap. J.*, **241**, 637.
Stauffer, J. 1980, *Ap. J.*, **85**, 1341.
Strom, S. E., Strom, K. M., and Carrasco, L. 1974, *Pub. A.S.P.*, **86**, 798.
Struve, O., and Rudkjøbing, M. 1949, *Ap. J.*, **109**, 92.
Ulich, B. L., and Haas, R. W. 1976, *Ap. J. Suppl.*, **30**, 247.
Vrba, F. J., Strom, K. M., Strom, S. E., and Grasdalen, G. L. 1975, *Ap. J.*, **197**, 77 (VSSG).
Walker, M. F. 1959, *Ap. J.*, **130**, 57.
Whittet, D. C. B. 1974, *M.N.R.A.S.*, **168**, 371.
_____. 1981, *M.N.R.A.S.*, **196**, 469.
Whitworth, A. 1979, *M.N.R.A.S.*, **186**, 59.
Wielen, R. 1971, *Ap. Space Sci.*, **13**, 300.
Wilking, B. A. 1981, Ph.D. thesis, University of Arizona.
Wilking, B. A., Lebofsky, M. J., and Rieke, G. H., and Kemp, J. C. 1979, *A.J.*, **84**, 199.

CHARLES J. LADA: Steward Observatory, University of Arizona, Tucson, AZ 85721

BRUCE A. WILKING: Department of Astronomy, The University of Texas, Austin, TX 78712